HHS Public Access

Author manuscript

Biochim Biophys Acta Mol Basis Dis. Author manuscript; available in PMC 2024 October 01.

Published in final edited form as:

Biochim Biophys Acta Mol Basis Dis. 2023 October ; 1869(7): 166811. doi:10.1016/j.bbadis.2023.166811.

Farnesoid X receptor activation inhibits pancreatic carcinogenesis

Zhen Xu[1,2,*], **Zhenhua Huang**[1,2,*], **Yifan Zhang**[1,2], **Haitao Sun**[1,2], **Ulf Hinz**[1], **Ulrike Heger**[1], **Martin Loos**[1], **Frank J. Gonzalez**[4], **Thilo Hackert**[1], **Frank Bergmann**[3,+], **Franco Fortunato**[1,2,+]

[1]Department of General, Visceral and Transplantation Surgery, University Hospital Heidelberg, Heidelberg, Germany.

[2]Section Surgical Research, University Hospital Heidelberg, Heidelberg, Germany.

[3]Institute of Pathology; University Hospital Heidelberg, Heidelberg, Germany.

[4]National Cancer Institute, National Institutes of Health, Bethesda, USA

Abstract

Farnesoid X receptor (FXR), a member of the nuclear receptor superfamily that controls bile acid (BA) homeostasis, has also been proposed as a tumor suppressor for breast and liver cancer. However, its role in pancreatic ductal adenocarcinoma (PDAC) tumorigenesis remains controversial. We recently found that FXR attenuates acinar cell autophagy in chronic pancreatitis resulting in reduced autophagy and promotion of pancreatic carcinogenesis. Feeding Kras-p48-Cre (KC) mice with the BA chenodeoxycholic acid (CDCA), an FXR agonist, attenuated pancreatic intraepithelial neoplasia (PanIN) progression, reduced cell proliferation, neoplastic cells and autophagic activity, and increased acinar cells, elevated pro-inflammatory cytokines and chemokines, with a compensatory increase in the anti-inflammatory response. Surprisingly, FXR-deficient KC mice did not show any response to CDCA, suggesting that CDCA attenuates PanIN progression and decelerate tumorigenesis in KC mice through activating pancreatic FXR. FXR is activated in pancreatic cancer cell lines in response to CDCA *in vitro*. FXR levels were highly increased in adjuvant and neoadjuvant PDAC tissue compared to healthy pancreatic tissue,

Corresponding authors: Franco Fortunato, University Clinic Heidelberg, Department of Surgery/Section Surgical Research, Im Neuenheimer Feld 365, 69120 Heidelberg, Fax: +49 (6221)-56 6830, Franco.Fortunato@uni-heidelberg.de.

*These authors contributed equally

+Shared senior authorship

Author contributions

F.F., T.H. and M.L. undertook the design of the study. Z.X., Z. H., Y.Z., H.S. U.H. and F.F. performed all the experiments. Pathology of animal tissues was undertaken by F.B. Statistics was undertaken by U.H. F.J.G. and F.F. The manuscript was written by Z.X., Z.H., T.H., M.L., F.J.G. and F.F. All reviewed the data, read the manuscript, and agreed with this version for submission.

Declaration of interests

The authors declare that they have no known competing financial interests or personal relationships that could have appeared to influence the work reported in this paper.

Conflict of interest

The authors declare that they have no conflict of interest.

indicating that FXR is expressed and potentially activated in human PDAC. These results suggest that BA exposure activates inflammation and suppresses autophagy in KC mice, resulting in reduced PanIN lesion progression. These data suggest that activation of pancreatic FXR has a protective role by reducing the growth of pre-cancerous PDAC lesions in response to CDCA and possibly other FXR agonists.

Introduction

Pancreatic ductal adenocarcinoma (PDAC) is currently the fourth leading cause of cancer-related deaths for both sexes and is expected to become the second most common cause of cancer-related mortality in developed countries within the next decade [1]. The five-year survival for pancreatic cancer patients remains as low as 11% in the USA. While surgical techniques and systemic chemotherapy have been improved, the overall five-year survival rate has remained virtually unchanged over recent decades [1–4]. New targets for early diagnosis or prevention of tumorigenesis progression are needed to improve survival.

Facing genetic pressure or environmental stress, one very early alteration in pancreatic cells is acinar-to-ductal metaplasia (ADM). This reprogramming progresses to pancreatic intraepithelial neoplasia (PanIN), the most common pancreatic precursor lesion. PanIN lesions are thought to be derived from ADM and can further develop into invasive tumor cells [5–8]. ADM and PanIN can be detected in chronic pancreatitis and the area adjacent to PDAC [9, 10]. Genetic mutation or tissue microenvironment pressure can cause acinar cell injury, potentially facilitating cellular ADM [11]. The precursor lesions progress from PanIN-1 (hyperplasia) to PanIN-2 (atypia), to PanIN-3 (carcinoma in situ) [12, 13]. A unique mutation in pancreatic Kras was sufficient to initiate PanIN lesions in a genetically engineered mouse model (GEMM) [14].

In recent years, bile acids (BAs) and the farnesoid X receptor (FXR) have become a major focus for modulating tumorigenesis [15, 16]. FXR appears to impair the tumor development in breast cancer (BC), hepatocellular carcinoma (HCC), and colorectal carcinoma (CRC), acting as a potential tumor suppressor [15, 17–20]. Its role in PDAC has also gained attention since FXR is highly expressed in pancreatic cancer tissue, correlating with nodal metastasis and poor prognosis [20]. A recent study found elevated serum BA/cholic acid derivates in PDAC patients with or without obstructive jaundice, suggesting that BAs promote carcinogenesis in PDAC patients [21]. While multiple studies indicate that FXR promotes PDAC cancer cell proliferation and progression, one study found an association with low-grade tumors and better survival [22]. While HCC and CRC experimental studies using FXR-deficient mice showed a tumor suppressor function for FXR, the precise role of FXR and BAs in pancreatic tumorigenesis remains unclear [16, 23]. Some studies reported the anti-tumorigenic effects of BAs, others reported pro-tumorigenic properties [24–26]. FXR was recently found to be highly increased in human and murine pancreatitis tissue and deletion of pancreatic FXR appeared to protect against caerulein-induced pancreatitis [27]. Since BAs may reflux into the pancreas duct and could contribute to common etiologies for biliary pancreatitis, their underlying mechanisms in pancreatic pathogenesis requires further study [28, 29].

FXR can also suppress the pancreatic autophagy by reducing the expression of autophagy-related protein-7 (Atg7) and lysosomal-associated membrane protein 2 (Lamp-2), thereby reducing autophagy activity in response to BA [30–33]. Our previous study showed increased FXR expression in human chronic pancreatitis tissue along with increased BA levels [34]. FXR can regulate autophagy signaling in both hepatocytes and mouse liver by suppressing the transcription of autophagy genes, and inhibiting the autophagic degradation progress [32]. We previously showed that both glycochenodeoxycholic acid (GCDC) and taurocholic acid (TCA) can activate nuclear FXR thereby suppressing autophagy function in AR42J cells *in vitro* [34]. As endogenous FXR agonists with different affinities and activation efficiencies for FXR, the order of potency for BAs is chenodeoxycholic acid (CDCA) > lithocholic acid (LCA) = deoxycholic acid (DCA) > cholic acid (CA) [35].

In this study, we show that CDCA feeding in mice suppresses autophagy signaling in the presence of FXR, activates the pancreatic inflammatory responses, and suppresses the production of PanIN lesions and the progression into invasive metaplasia in PDAC. FXR is also highly activated in chemo-naive and neoadjuvant human PDAC patients without any correlation between their FXR profile and survival.

Materials and methods

Cell Culture

AR42J, CAPAN-1 and PANC-1 cells were purchased from ATCC and cultured under conditions recommended by the ATCC in F-12, DMEM or IMDM Medium with 10 – 20% FBS, 50 μg/ml streptomycin, 50 U/ml penicillin G and 2.5 mg/ml plasmocin. The cell lines were grown in 75 cm^2 flasks and the medium was renewed every 3 to 4 days, the cells were sub-cultured when approximately 90% confluent. AR42J cells were also cultured in Matrigel and fixed with 4% paraformaldehyde (PFA) for 2 hours at room temperature in a fume hood. Using HistoGel to embed Matrigel to form a sandwich and then transferred into the tissue blocks to make formalin-fixed paraffin-embedded (FFPE) tissue samples for single layer cell immunofluorescence staining. CAPAN-1 and PANC-1 were also fixed with 4% PFA and processed as described for AR42J cells.

Antibodies and reagents

Antibodies were selected according to proven functionality for use with formalin-fixed paraffin-embedded (FFPE) tissue sections and western blots by as revealed in previously published studies or antibody test as described previously [10, 34, 36, 37]. All antibodies used in this investigation are listed in the Supplemental Materials (Table 1–4).

Human subjects

This study was approved by the Ethics Committee of Heidelberg University (Ethics Committee Approval No. S-199/2017 and S-708/2019), cording to the Helsinki Declaration. The tissue samples are from the tissue bank of the Department of Surgery in Heidelberg University. All of the patients had been informed and signed formal consents for use of their tissues for scientific research. In total, 36 tissue samples from patients characterized previously were used, which included 18 tissue samples from patients after neo-adjuvant

therapy, 9 adjuvant chemo-naïve tissue samples from resectable PDAC patients undergoing surgery, and 9 normal pancreata from healthy organ donors without appropriate recipients found for transplantation [37].

Animals

LSL-Kras^{G12D} mice: Exon1 of Kras was flanked by loxp-stop-loxp and exon1 containing G12D, were kindly provided by David Tuveson [14]. *Fxr*$^{F/F}$ mice, in which the last *Fxr* exon of was flanked by two loxP sites, were described previously [38]. In p48-cre mice, part of p48 locus was replaced by the Cre recombinase gene [39]. LSL-*Kras*^{G12D} mice were crossed with p48-cre mice to generate p48-Cre; LSL-*Kras*^{G12D} mice (KC mice). *Fxr*$^{F/F}$ mice were crossed with p48-cre mice to generate Fxr-Cre mice (FC mice). KC mice were crossed with *Fxr*$^{\Delta pan}$ mice to generate Fxr-Cre; p48-Cre; LSL-*Kras*^{G12D} mice (KFC mice). The mice were bred under standard conditions in a pathogen-free facility. All mouse strains were established and maintained with a C57LB/6J background. All animal studies were approved (study # G-24/17) by the Institutional Animal Care and Use Committee of Heidelberg University in accordance with the Federal Presiding Board guidelines for Animal Care, Karlsruhe, Germany.

Experiment design

Twenty-three-week-old male mice were administrated 0.1% (w/w) CDCA solved in PBS in the drinking water for 8 weeks, the vehicle control groups were given the same concentration of PBS in drinking water. KC mice exposed to CDCA are referred to as KC-CDCA mice, while KC-PBS designate normal feeding mice in which PBS was added to the drinking water. The same rule was applied for KFC mice to categorize KFC-PBS and KFC-CDCA. Mice were killed at age 30-weeks and the whole pancreas tissue was resected as described previously [10, 40, 41]. The pancreas was washed in cold PBS for a few seconds, then weighed. The tissue was cut into two pieces; one piece was immersed in liquid nitrogen and kept at −80°C and another piece was soaked in 4% phosphate-buffered formaldehyde solution.

Cell viability assay

Cell viability was measured by the MTT assay. Two-hundred μl of medium containing 5×10^3 AR42J, CAPAN-1 or PANC1 cells were plated in 96-well plates, 6 wells per group. After growing for 24 h, the cells were treated with different concentration of CDCA with each group having the same concentration of DMSO (vehicle). Twenty-four h later, 10 μl MTT solution (5 mg/ml) were added into each well and after incubating for 4 hours, the medium was discarded and 100 μl DMSO added to dissolve the MTT formazan crystals. After the MTT formazan crystals were completely dissolved, the 96-well plate was placed in a microplate spectrophotometer and absorbance of 570 nm and 690 nm measured. The viability was assessed by the formula: (Treatment OD - blank OD) / (Control OD – blank OD) x 100%.

Genotyping

DNA extraction was performed according to the protocol supplied with the Fast Tissue-to-PCR Kit using mouse tails. Two μl DNA extract was added to a 20 μl PCR reaction system containing Dream Taq PCR Master Mix primers and nuclease-free water (Thermo Fisher Scientific, Waltham, MA, USA). DNA amplification was conducted in a real-time quantitative PCR machine (LifeTouch and Eppendorf PCR cycler), followed by separation on a 2% agarose gel containing DNA Stain G (SERVA, Heidelberg, Germany) under standard DNA electrophoresis conditions and UV illuminator visibility. The primers used in the PCR reaction are listed: Kras forward primer: 5'-CCTTTACAAGCGCACGCAGACTGTAGA-3', reverse primer: 5'-AGC-TAGCCACCATGGCTTGAGTAAGTCTGCA -3'; p48-cre forward primer: 5'-ACC-GTCAGTACGTGAGATATCTT-3', reverse primer: 5'-ACCTGAAGATGTTCGCGA-TTATCT-3'; Fxr forward primer: 5'-ACAAGAGCCCTGTAAAGAGTTTTC-3', Fxr reverse primer: 5'-GTGAGGAAGATGACAAAATTGCTAC-3'.

Histopathological evaluation

Hematoxylin & eosin (H&E) staining was performed on fixed mouse tissues. Tissue sections with H&E staining were examined by a pathologist who was blinded to the exact identity of each sample. Histopathological evaluation including normal acinar cells, islets, ADM, PanIN-1, PanIN-2, PanIN-3 and stroma were performed. Annotations for different parts were draw by manual comprehensively. With the Tissue Gnostics imaging and StataQuest systems, a specific area of each part was analyzed based on the exact area data from the whole tissue, which is a more precise comparison to selected microscope field of view.

Normal acinar cells are enzyme secreting units, so called acini. Acinar cells are pyramidal-shaped and polarized in which endoplasmic reticulum occupy the basal pole and zymogen granules occupy the apical pole. ADM cells are derived from acinar cells with loss of cytoplasmic proteins, and thus a ductal cells morphology is shown with cytoplasm contraction. PanIN-1 consist of flat epithelium composed of tall columnar mucin and round and oval nuclei, located on the base side. PanIN-2,3 is an atypical form with papillary mucin cells, nuclear enlargement with crowing. Pseudostratification was found along with loss of polarity in cytoplasm [12]. Representative images are shown in Suppl. Figure 2.

Real-time PCR

Frozen whole mouse pancreatic tissues were extracted using TRIzol-Reagent (Life Technologies, Invitrogen) and processed, as described previously [10, 34]. The primer sequences for mouse have been previously reported and were additionally checked using NCBI primer blast [42]. FXR Primer sequences in real-time PCR analysis Forward: CTTGATGTGCTACAAAAGCTGTG; Reverse: ACTCTCCAA-GACATCAGCATCTC, against GAPDH Primer sequences Forward: TGACCTCAA-CTACATGGTCTACA; Reverse: CTTCCCATTCTCGGCCTTG.

Immunofluorescence (IF)

IF was conducted using FFPE pancreatic tissue sections and performed as described in detail previously [10, 34, 36, 37] IF images were acquired from the integral tissue sections

automatically with a fluorescence microscope (Observer. Z1, Zeiss) under the control of the TissueFAXS software (TissueGnostics, Vienna, Austria). Appropriate exposure time and sensitivity threshold were set to different channels (DAPI, Cy3.5 [570 nm] and Cy5 [650 nm], Chroma Technology, USA) to detect different target proteins. The TissueFAXS system can also be used to acquire the H&E staining. The images were analyzed by the StrataQuest software (TissueGnostics), which can detect the location, intensity of target fluorescence signals, and quantitation of the total cell numbers from DAPI positive cells or target-protein positive cells carried out. To achieve optimal cell detection, nuclei size and cellular mask size were adjusted for different targets.

For the evaluation of positive cells, FACS-like scattergrams were created, in which all cells were plotted based on their IF mean intensity versus the DAPI mean intensity. An appropriate cutoff was applied to categorize specific IF-positive signals in cells, according to cell size and the intensity of target-protein in negative controls, with the real-time back gating function of the software. Expression levels of the specific target proteins were demonstrated by the percentage of target protein-positive cell numbers and total DAPI positive cell-numbers within the entire tissue, which can be adopted from the upper-right quadrant in a FACS-like scattergrams approach, as described before [10, 34, 36, 37]. For MPO positive cells, we determined the number of MPO-positive cells within the total DAPI-positive cell numbers in the entire tissue (cell number per mm^2) [10, 37]. Similarly, the colocalization of different proteins with acinar cell marker α-amylase or duct-like cell and neoplastic cell marker CK19 were analyzed with StrataQuest software [40]. CK19 is a useful marker for staining ductal-like cells and is also detects cells of early neoplastic transformation and was used to discriminate between the normal and neoplastic cells [43].

Western blotting (WB)

Mouse pancreas tissues were homogenized in ice-cold lysis buffer (50 mM HEPES, 5 mM CHAPS, 5 mM DTT), with the addition of proteinase inhibitors (aprotinin, leupeptin, pepstatin, PMSF) and a trypsin inhibitor before use. The proteins were collected and the concentrations were measured with the BCA Protein Assay Kit according to the manufacturer's instructions. Mini-Protean® 3 Cell System and SDS-polyacrylamide gels were used to perform electrophoresis. The transfer procedure was performed in ice-cooled transfer buffer by the Mini Trans-Blot Cell System. The membranes were scanned with the ODYSSEY® CLx (LI-COR) imaging systems, and the digital images were captured. ImageJ software was adopted for quantification of the target-protein.

Statistical Analysis

The software GraphPad Prism 6 was applied for the statistical analysis. All quantitative data were presented as mean ± SEM (Standard Error of the Mean). Analysis of variance (ANOVA) was applied for statistical analysis for multiple groups analysis, followed by Student's t-Test for two groups analysis. The outlier identification was performed for the data enrolled. Results with p value ≤ 0.05 were considered to be statistically significant. The significance score was shown as: *< 0.05; **< 0.01; ***< 0.001; ****< 0.0001.

Results

Generation of *Kras-p48Cre* and *Kras-Fxr-p48Cre* mice

To investigate FXŔs role in pancreatic carcinogenesis, we crossed *Kras-p48Cre* (KC) mice with pancreas-deficient-*Fxr*-floxed mice resulting in *Kras-Fxr-p48Cre* (KFC) mice in which *Fxr* is disrupted in the pancreas. PCR genotyping of *Kras*, pancreas associated transcription factor 1a (*Ptf1a*, *p48)-Cre*, and *Fxr* was performed on genomic DNA extracted from mouse ears. The $Kras^{G12D}$ mutation is represented by a 550 bp fragment, and *p48-Cre* by a 350 bp fragment. Wild-type *Fxr* had a 378 bp fragment, while the $Fxr^{F/F}$ allele was represented by a 458 bp fragment. Two fragments (378 and 458 bp) were present in heterozygous $Fxr^{+/-}$ mice (Suppl. Fig. 1A). Since FXR is absent in the pancreas but expressed in the liver, the Cre system is sufficient to deplete pancreatic FXR [44]. Mouse pancreata were harvested, processed in formalin-fixed and paraffin-embedded (FFPE) tissue and hematoxylin and eosin (H&E) stained, as described previously [34, 36]. In $Fxr^{F/F}$ and $Fxr^{\Delta pan}$ mice, the pancreas appeared normal with normal acini, islets, ductal structures, and blood vessels. Pancreas-specific FXR deficiency did not alter any phenotype in the pancreas (Suppl. Fig. 1B). This result is consistent with a recent study suggesting that pancreatic *Fxr* disruption did not directly induce alterations in pancreatic histology and exocrine function under normal conditions [27]. KC mice showed ADM and PanIN progression over time. At 30 weeks, the KC mice had residual acinar cells, ADM, PanINs, and massive stroma in their pancreas [45]. At 45 weeks of age, fewer acinar cells remained, and a higher PanIN proportion was observed. Morphology as revealed by H&E staining, was similar in KC and KFC mice (Suppl. Fig. 1C). While KC and KFC mice showed the well-described pancreatic cells neoplasia of ADM and PanIN-like morphology, pancreatic FXR deficiency caused no notable morphological changes.

Physiological properties were unaffected after BA exposure

Twenty-three-week-old KC or KFC mice were given 0.01 % (w/w) CDCA in the drinking water for eight weeks (Fig. 1A). The control group's drinking water contained the same concentration of phosphate-buffered saline (PBS). The body weight of a healthy 32-week-old mice was 36.7 ± 3.7 g (mean ± standard error of the mean [SEM]). The pancreata were enlarged in the KC and KFC mice, however, they remained normal in *Kras-Fxr* WT and $Fxr^{\Delta pan}$ mice (Fig. 1B). At 30 weeks, the body weights did not differ between the KC-PBS and KFC-PBS, KC-CDCA, and KFC-CDCA groups (five mice per group) (Fig. 1C). In addition, the pancreas weights did not differ significantly among the four treatment groups (Fig. 1D). Moreover, the ratios of pancreas weight/body weight were higher in the KC than in the KFC mice with or without CDCA. CDCA feeding decreased the pancreas to body weight, ratio indicating that FXR deficiency may attenuate BA tolerance (Fig. 1E). This result suggests that FXR levels are elevated in pancreatic pre-tumorigenic cells and do not strongly influence the pancreatic physiological response to CDCA.

BA feeding inhibits pancreatic precursor lesion progression in KC mice.

Spontaneously pancreatic ADM and PanIN were found in KC mice as early as eight weeks of age, and the precursor lesions continue to progress over time. In high-grade lesions, fewer normal acinar cells remained, and more ADMs and PanIN lesions were observed

(Suppl. Fig. 2A–B). H&E imaging with the TissueFAXS system, and pathological analysis was performed using the StrataQuest software (Suppl. Fig. 2C–D). Each lesioń s area in the integral tissue was annotated and its proportion was calculated with the Tissue Gnostics imaging and StataQuest systems. KC mice fed with CDCA had significantly more acinar cells ($p = 0.0168$) and fewer PanIN-1 lesions ($p = 0.0357$) than KC mice fed PBS but had similar PanIN-2 and PanIN-3 lesions ($p = 0.1404$) (Suppl. Fig. 2E). Surprisingly, ADM development did not differ. Fewer PanIN precursor lesions and more acini cells were detectable after CDCA feeding with intact FXR receptor.

BA feeding improves pancreatic neoplasia and fibrogenesis in KC mice with intact FXR.

Quantitative immunofluorescence (IF) analyses for α-amylase (intact acini) and keratin-19 (KRT19/CK19; pan-neoplastic cells) cells were consistent. In KRAS-FXR floxed WT mice, α-amylase was present and levels were not changed by CDCA feeding. In the normal pancreas of KrasFXR floxed mice, CK19 was only detectable in 3% of mostly ductal cells and few neoplastic cells within the entire pancreatic tissue but decreased to 1% after by exposure to CDCA with intact FXR (Suppl. Fig. 3A–B). However, KC-CDCA mice had significantly more α-amylase-positive acinar cells than KC-PBS mice ($p = 0.047$). FXR-deficient mice tended to have more α-amylase-positive acinar cells, but the difference did not reach statistical significance (Fig. 2A–B). In contrast, KC mice exposed to CDCA had significantly fewer CK19-positive neoplastic cells than KC mice fed PBS ($p = 0.0317$) (Fig. 2C–D). Interestingly, CK19-positive cell numbers in KFC mice did not significantly differ between CDCA or PBS exposure. This result suggests the presence of lower ductal epithelial cell transformation in KC mice after exposure to CDCA.

The proliferation marker Ki67 was also reduced in KC mice after CDCA feeding, suggesting reduced epithelial cell proliferation (Fig. 2E). We found no alteration in pancreatic-FXR-deficient KFC mice after CDCA feeding suggesting that CDCA reduces pancreatic PDAC desmoplasia with intact FXR, while FXR loss does not alter pancreatic neoplasia. *Fxr* mRNA levels were measured in wild-type and *Kras-p48-Cre* mice with or without CDCA feeding. While *Fxr* mRNA was elevated in KC mice with or without CDCA administration, it was non-significantly increased after CDCA feeding (Suppl. Fig. 3C).

Pancreatic stellate cells (PSCs) are known to be involved in stroma formation and neoplasia. PSC proliferation was detected by measurement α-smooth-muscle actin (ACTA2) levels. IF staining and quantitative analysis showed that KC mice administrated CDCA had fewer ACTA2-positive cells than control mice ($p = 0.0314$). No difference in ACTA2 was found in pancreatic FXR-deficient KFC mice after CDCA exposure, suggesting that intact FXR attenuates pancreatic neoplastic lesions and improves pancreatic desmoplasia in response to BAs (Fig. 2F–G).

BA feeding inhibits autophagy in KC mice.

Autophagy is a critical cellular degradative pathway for maintaining pancreatic cellular homeostasis. However, whether impaired autophagy is a cause or consequence of pancreatic damage remains unclear. Impaired autophagy signaling promoted chronic pancreatitis development and increased ADM formation in a mouse model [10, 46, 47]. In the Kras-

derived PanIN murine model (KC mice), as a self-digestion metabolic pathway, a high autophagy level can promote tumor growth [48]. FXR was shown to be a potent autophagy suppressor [32, 34]. To investigate whether autophagy was altered by CDCA feeding, total pancreas protein extract was used for LAMP2, autophagy-related 5 (ATG5), and light-chain 3 (LC3) immunoblotted analysis with GAPDH as a loading control (Fig. 3A). Additionally, we performed immunoblot analysis against SQSTM1 (p62) (Fig. 3B). The gray-scale values of fragments for four mice per group were calculated using the ImageJ software. The normalized values for LAMP2 ($p = 0.0121$), LC3 ($p = 0.0165$), ATG5 ($p = 0.0057$) were all reduced while the expression of the autophagy substrate p62 ($p = 0.0222$) was increased in KC mice exposed to CDCA (Fig. 3C–F). No autophagy alterations were found in KFC mice with or without CDCA feeding. Consistent with a recent report, FXR activation by CDCA reduced pancreatic autophagy signaling in KC mice [27].

Pro-inflammatory cytokines and chemokines are elevated by BA feeding in KC mice.

The inflammatory response in the pancreas may have both pro-tumorigenesis and anti-tumorigenesis properties. The activated inflammatory response in acinar cells is protective against endogenous pressure or stimuli [36]. Pro-inflammatory cytokines and chemokines, including tumor necrosis factor-alpha (TNF-α), interleukin-6 (IL-6), and monocyte chemoattractant protein 1 (MCP-1) were examined in pancreatic tissue by IF staining, Quantitative analysis of cytokines and chemokines in acinar cells was based on their colocalization with α-amylase.

TNF-α ($p = 0.0019$) and IL-6 ($p = 0.0386$) levels were significantly higher in the α-amylase-positive acinar and neoplastic cells of KC mice given CDCA with pre-cancerous precursor lesions. In contrast, they were unchanged in KFC mice (Fig. 4A–D). Precursor lesions and stroma occupy most pancreatic tissue of KC mice at the age of 30 weeks (Suppl. Fig. 1C), and pancreatic cancer showed little immunogenic response. We predict that most α-amylase-negative cells are somehow neoplastic cells. Interestingly, those α-amylase-negative and presumably neoplastic cells are more capable of responding to TNF-α and IL-6 in response to CDCA.

Similarly, MCP-1 ($p = 0.0493$) and myeloperoxidase (MPO; $p = 0.0422$) levels were higher in KC mice fed CDCA and KFC mice with or without CDCA. Pro-inflammatory signals also tended to increase in FXR-deficient mice but did not differ with or without CDCA. MCP1 levels did not differ in neoplastic cells with a similar α-amylase level (Fig. 4E–H). These results indicate that CDCA increased pro-inflammatory cytokines, chemokines, and MPO levels in KC mice, reducing their overall neoplastic activity, suggesting that an increased inflammatory response may promote FXR's cytoprotective effect in response to CDCA.

The anti-inflammatory response was activated in KC mice by BA administration

Transforming growth factor-beta (TGF-β), an important regulator of the anti-inflammatory response and fibrosis, was investigated by IF [49]. TGF-β levels were increased in acinar cells of KC mice ($p = 0.0309$) but decreased in KFC mice in response to CDCA feeding (Fig.

5A–B). α-Amylase-negative and presumably neoplastic cells appeared to produce higher TGF-β levels with and without CDCA.

Another anti-inflammatory cytokine interleukin 10 (IL-10) was examined to elucidate the anti-inflammatory response. CDCA increased IL-10 levels compared to normal control in KC mice ($p = 0.0232$) (Fig. 5C–D). Interestingly, α-amylase-negative and presumably neoplastic cells produced 6- to 8-fold higher IL-10 levels, which were slightly higher after CDCA exposure. IL-10 tended to have non-significantly higher levels in response to CDCA. These results on TGF-β and IL-10 levels suggest that the anti-inflammatory response was activated by CDCA in KC but not KFC mice.

BA exposure activates FXR signaling in pancreatic tumor cells

We previously showed that FXR expression was induced in AR42J acinar-like cells by exposure to TCA and GCDC [34]. Among all BAs, CDCA was the most potent FXR ligand, with relatively low cytotoxicity. However, CDCA was cytotoxic to AR42J cells with a half-maximal inhibitory concentration (IC50) of 255 μM; MTT-assay-based cell viability was unchanged at higher concentrations. Similar MMT assay results were obtained with the CAPAN-1 and PANC-1 pancreatic cancer cell lines (Fig. 6A). Since AR42J cells tend to grow in clusters, they were cultured and treated with CDCA in Matrigel and made into 4 μm-thick FFPE slides to examine the cell layer (Fig. 6B). IF quantitation showed significantly increased nuclear FXR levels after treatment with 200 μM CDCA (Fig. 6C). We further confirmed that 200 μM CDCA increased nuclear FXR levels in human PANC-1 and CAPAN-1 pancreatic cancer cell lines as revealed by IF (Fig. 6D–E and Suppl. Fig. 4). These data suggest that CDCA exposure increases nuclear FXR levels in pancreatic cancer cells.

FXR is highly elevated in chemo-naïve adjuvant and neoadjuvant human PDAC tissue

FXR is highly expressed in chronic pancreatitis and metastatic PDAC [34, 50]. FXR was co-stained with CK19 in neoadjuvant and adjuvant chemo-naïve PDAC patients and donated healthy pancreatic tissues by IF (Fig. 7A). FXR levels in neoplastic cells were 16-fold higher in chemo-naïve adjuvant ($p = 0.0060$) and 82-fold higher in neoadjuvant ($p < 0.0001$) PDAC tissues compared to healthy tissue. FXR levels were also five-fold higher in neoadjuvant ($p = 0.0008$) compared to chemo-naïve adjuvant tissues (Fig. 7B). These results suggest that chemo-naïve adjuvant and neoadjuvant PDAC patients have significantly higher FXR levels than healthy individuals, which are even higher in patients exposed to chemotherapy.

Discussion

This study provides evidence for the first time that in KC mice CDCA activates FXR in the pancreas and reduces pancreatic carcinogenesis. Therefore, activation of FXR showed tumor-suppressive properties. Consistent with our findings, FXR is highly increased in human and murine pancreatitis tissue, and loss of pancreatic FXR protects against caerulein-induced pancreatitis [27]. While some studies have found FXR to be associated with poor prognosis, others revealed a better survival rate is positively correlated with higher FXR expression [22, 50, 51]. In the present study, FXR levels were five-fold higher in

tissues from neoadjuvant patients than from chemo-naïve adjuvant PDAC patients. This finding indicates that cytotoxic anti-cancer therapy increased FXR expression, which is correlated with regulation of the detoxifying enzyme cytochrome P450 family 3 subfamily A members (CYP3As) [30]. FXR levels were 82-fold higher in neoadjuvant and 16-fold higher in chemo-naive adjuvant tissues compared to healthy donor tissues, indicating that neoplastic conditions are sufficient to activate FXR expression. FXR also regulates CYP3A4, potentially explaining the higher FXR levels found in neoadjuvant PDAC patients [30].

Mice lacking FXR spontaneously developed liver cancer indicating that FXR suppresses tumorigenesis in HCC likely due to increased cholestasis [15, 52]. Other studies also found that FXR impaired tumor-promoting functions in breast cancer, HCC, and CRC, acting as a tumor suppressor in agreement with our results [15, 17–20, 23].

FXR is the main regulator of BA functional effects in humans. Chronic pancreatitis is a risk factor for PDAC development, and previous studies revealed that FXR is increased in chronic pancreatitis [34]. The present study showed that nuclear FXR levels are highly elevated in chemo-naïve tissues of PDAC patients and even more so after neoadjuvant therapy. However, our cohort did not include PDAC patients with metastases. Further clinical studies and basic investigations are needed to fully elucidate the association between FXR and PDAC carcinogenesis. Notably, FXR levels were elevated in KC mice fed a PBS solution without CDCA, indicating that the development of PDAC precursor lesion ADMs and PanINs is sufficient to activate FXR expression under neoplastic conditions.

Increased serum BA levels had tumorigenic potential in breast and gastrointestinal cancer. [15] However, BAs' roles in PDAC remain controversial, with promoting and suppressing PDAC properties having been reported [15, 21]. The different responses of cancer cells to BAs appear to depend on their individual FXR expression profiles [15]. PanIN lesions are the most common and best-characterized pancreatic precursor metaplasia in PDAC tissue. Several mouse models have been established to recapitulate the spectrum from PanIN lesions to PDAC tumorigenesis [53]. Here, as a PanIN precursor model, KC mice developed early ADMs as a precursor metaplasia for PanIN that were detectable by H&E staining at four weeks old, with PanIN lesions becoming visible at eight weeks old. Consistent with previous studies, the KC mice generated for this study showed severe neoplastic ductal structures at 30 weeks old. PanIN-1 lesions replaced around 60% of the pancreas. Compared to normal feeding, KC mice fed BAs had less metaplasia, with more acinar cells and fewer ductal cells, and decreased neoplastic cell proliferation, suggesting a suppressive effect on PanIN progression for BAs. In our experimental mouse model, disruption of pancreatic FXR alone did not influence pancreatic histology or exocrine function, which was recently confirmed [27].

The inhibition of PanIN progression in KC mice after BA/CDCA feeding might be associated with the attenuation or enhancement of Kras-driven molecular changes in autophagy signaling, fibrogenesis, and inflammation responses, all of which are involved in PanIN progression. Kras-driven mouse tumors show increased basal autophagy and inhibition of autophagy suppresses tumor cell proliferation and inhibits tumorigenesis

progression [54, 55]. The present study revealed that LAMP2, ATG5, LC3 and p62 levels indicate that CDCA feeding inhibited autophagy activity in KC mice as indicated by measurement of LAMP2, ATG5, LC3 and p62 protein levels, suggesting that decreased autophagy signaling may contribute to inhibiting PanIN-1 development and thus progression of the whole PanIN lesion spectrum. CDCA is one of the most potent FXR agonists and it is likely that FXR activation in the pancreas mediates these effects [23]. Along with autophagy signaling, tumor growth is interconnected with the balance of cell growth and cell death. We observed less proliferation (Ki67) and fewer neoplastic cells (CK19) in accordance with more α-Amylase positive acinar cells in the KrasCre mouse pancreas after exposure to CDCA compared to control KrasCre mice, suggesting that exposure of mice with intact FXR receptor to bile acid FXR-activators reduce tumorigenesis. Cell death by apoptosis and necroptosis really did not show any difference after CDCA feeding, we predominantly determine less cell proliferation and no strong induction of apoptosis (Suppl. Fig. 5A/B). We conclude that CDCA feeding with intact FXR show rather sign of reduced tumor cell growth and reduced tumorigenesis.

Acinar cells can produce cytokines and chemokines in response to an insult and could regulate immune cell infiltration. The pro-inflammatory response in acinar cells can play a protective role in eliminating damaged cells and initiating tissue repair to restore homeostasis [36, 56, 57]. The early-phase inflammatory mediator TNFα and late-phase inflammatory mediator IL-6 levels were elevated in KC mice in response to CDCA. Consistent with the TNF-α and IL-6 data, MCP-1 and MPO were increased after BA exposure, indicating greater monocyte infiltration. No alterations were detected in KFC mice, suggesting that inflammation activation by CDCA is FXR-dependent. Importantly, KC mice with 30% CK19-positive neoplastic cells and fibrotic tissue could still produce cytokines in response to CDCA. While PDAC tissues showed low immunogenic responses with few infiltrated immune cells, neoplastic cells might still be able to produce inflammatory responses.

CDCA feeding upregulated the anti-inflammatory mediators TGF-β and IL-10, which both increase anti-inflammatory processes. This effect was suggested as a beneficial response to KRAS-driven pancreatic cell metaplasia [58]. Inflammation in the pancreas is enhanced by high RAS activity due to the *Kras*^{G12D} mutant, which maintains and promotes PanIN progression. However, the anti-inflammatory response is equally high [59]. This enhanced anti-inflammatory response, mediated by CDCA activation of FXR, might explain the acinar cell-protected phenotype caused by the reprogramming of acinar-ductal cells and, thus, inhibited ductal cell transformation.

In summary, this study showed that CDCA administration to KC mice increased the acinar cell tissue proportion and slowed PanIN progression by suppressing autophagy and fibrogenesis and activating the inflammatory response. This protective effect was not present in mice in the absence of FXR in the pancreas. Pancreatic neoplasia PDAC precursor lesions and established PDAC are sufficient to activate pancreatic FXR expression. Therefore, FXR could be a potential novel therapeutic target against pancreatic cancer.

Supplementary Material

Refer to Web version on PubMed Central for supplementary material.

Acknowledgements

The authors thank the service support from members of the European Pancreas Center (EPZ) - Biobank and PancoBank as well as the section of surgical research in Heidelberg: Sonja Bauer, Markus Fischer, Ingrid Herr, Ulf Hinz, Nathalia Giese, Karin Ruf, Miriam Schenk, Kathrin Schneider and Wolfgang Groß and Michael Schäfer for the IT support. Clinical data were kindly provided by Christine Tjaden and Ulf Hinz. We greatly appreciate the support of David Tuveson and Risa Karakida Kawaguchi for kindly providing the transgenic mice. This study was supported by the German Research Foundation (Deutsche Forschungsgemeinschaft, DFG) Excellent Initiative Frontier award to FF, and the affiliated people's Hospital of Jiangsu University and a stipend of China Scholarship Council to ZX and ZH. The Biobank of the European Pancreas Center (EPZ), Department of General Surgery, University Hospital Heidelberg, is supported by the Heidelberger Stiftung Chirurgie and the German Ministry for Education and Research (Bundesministerium für Bildung und Forschung, BMBF) grants 01GS08114 and 01ZX1305C to TH, Nathalia Giese, and Markus W. Büchler and the National Cancer Institute Intramural Research Program (FJG).

Zhen Xu is currently working for the Department of Oncology, the First Affiliated Hospital of Soochow University, Suzhou, Jiangsu, China. Zhenhua Huang is currently working for Department of General Surgery, Zhenjiang First People's Hospital, No. 8 Dianli Road, Runzhou District, Zhenjiang, Jiangsu, China. Thilo Hackert just start working for University Clinic Hamburg-Eppendorf/UKE, Klinik und Poliklinik für Allgemein-, Viszeral- und Thoraxchirurgie, Martinistraße 52, 20246 Hamburg.

Abbreviation

ADM	acinar-to-ductal metaplasia
Atg5	autophagy-related protein-5
BA	bile acid
BC	breast cancer
C57LB/6J	background wild-type mouse
CA	cholic acid
CDCA	chenodeoxycholic acid
CK19/Krt19	Cytokeratin/Kreatin 19
CRC	colorectal carcinoma
Cy5	Cyanine 5 monosuccinimidyl ester
DAPI	4',6-Diamidino-2-phenylindol)
DCA	deoxycholic acid
DMSO	Dimethylsulfoxid
FACS	fluorescence activated cell sorting
FC	Fxr-Cre mice
FFPE	formalin-fixed paraffin-embedded

FXR	Farnesoid X receptor
$Fxr^{\Delta pan}$	FXR is depleted in the pancreas
$Fxr^{F/F}$	Floxed Genotype
GCDC	glycochenodeoxycholic acid
GEMM	genetically engineered mouse
H&E	Hematoxylin & eosin
HCC	hepatocellular carcinoma
IF	Immunofluorescence
IL-6	interleukin-6
KC	Kras-p48Cre
Lamp-2	lysosomal-associated mem-brane protein 2
LC3	light-chain 3
LCA	lithocholic acid
LSL	loxp-stop-loxp
MCP-1	monocyte chemoattractant protein 1
MPO	Myeloperoxidase
MTT	3-(4,5-Dimethylthiazol-2-yl)-2,5-diphenyl-tetrazoliumbromid
NCBI	National Center for Biotechno-logy Information
PanIN	pancreatic intraepithelial neo-plasia
PBS	Phosphate Buffered Saline
PCR	polymerase chain reaction
PDAC	pancreatic ductal adeno-carcinoma
PSC	Pancreatic stellate cells
aSMA	α-smooth-muscle actin
TCA	taurocholic acid
TGFß	Transforming growth factor-beta
TNFα	tumor necrosis factor-alpha

References

[1]. Siegel RL, Miller KD, Fuchs HE, Jemal A, Cancer statistics, 2022, CA Cancer J Clin, 72 (2022) 7–33. [PubMed: 35020204]

[2]. Leinwand J, Miller G, Regulation and modulation of antitumor immunity in pancreatic cancer, Nat Immunol, 21 (2020) 1152–1159. [PubMed: 32807942]

[3]. Neoptolemos JP, Kleeff J, Michl P, Costello E, Greenhalf W, Palmer DH, Therapeutic developments in pancreatic cancer: current and future perspectives, Nat Rev Gastroenterol Hepatol, 15 (2018) 333–348. [PubMed: 29717230]

[4]. Siegel RL, Miller KD, Fuchs HE, Jemal A, Cancer Statistics, 2021, CA Cancer J Clin, 71 (2021) 7–33. [PubMed: 33433946]

[5]. Storz P, Acinar cell plasticity and development of pancreatic ductal adenocarcinoma, Nat Rev Gastroenterol Hepatol, 14 (2017) 296–304. [PubMed: 28270694]

[6]. Reichert M, Rustgi AK, Pancreatic ductal cells in development, regeneration, and neoplasia, J Clin Invest, 121 (2011) 4572–4578. [PubMed: 22133881]

[7]. Wang L, Xie D, Wei D, Pancreatic Acinar-to-Ductal Metaplasia and Pancreatic Cancer, Methods Mol Biol, 1882 (2019) 299–308. [PubMed: 30378064]

[8]. Wei D, Wang L, Yan Y, Jia Z, Gagea M, Li Z, Zuo X, Kong X, Huang S, Xie K, KLF4 Is Essential for Induction of Cellular Identity Change and Acinar-to-Ductal Reprogramming during Early Pancreatic Carcinogenesis, Cancer Cell, 29 (2016) 324–338. [PubMed: 26977883]

[9]. Hruban RH, Maitra A, Goggins M, Update on pancreatic intraepithelial neoplasia, Int J Clin Exp Pathol, 1 (2008) 306–316. [PubMed: 18787611]

[10]. Zhou X, Xie L, Xia L, Bergmann F, Buchler MW, Kroemer G, Hackert T, Fortunato F, RIP3 attenuates the pancreatic damage induced by deletion of ATG7, Cell Death Dis, 8 (2017) e2918. [PubMed: 28703808]

[11]. Houbracken I, de Waele E, Lardon J, Ling Z, Heimberg H, Rooman I, Bouwens L, Lineage tracing evidence for transdifferentiation of acinar to duct cells and plasticity of human pancreas, Gastroenterology, 141 (2011) 731–741, 741 e731–734. [PubMed: 21703267]

[12]. Basturk O, Hong SM, Wood LD, Adsay NV, Albores-Saavedra J, Biankin AV, Brosens LA, Fukushima N, Goggins M, Hruban RH, Kato Y, Klimstra DS, Kloppel G, Krasinskas A, Longnecker DS, Matthaei H, Offerhaus GJ, Shimizu M, Takaori K, Terris B, Yachida S, Esposito I, Furukawa T, Baltimore Consensus M, A Revised Classification System and Recommendations From the Baltimore Consensus Meeting for Neoplastic Precursor Lesions in the Pancreas, Am J Surg Pathol, 39 (2015) 1730–1741. [PubMed: 26559377]

[13]. Lennon AM, Wolfgang CL, Canto MI, Klein AP, Herman JM, Goggins M, Fishman EK, Kamel I, Weiss MJ, Diaz LA, Papadopoulos N, Kinzler KW, Vogelstein B, Hruban RH, The early detection of pancreatic cancer: what will it take to diagnose and treat curable pancreatic neoplasia?, Cancer Res, 74 (2014) 3381–3389. [PubMed: 24924775]

[14]. Hingorani SR, Petricoin EF, Maitra A, Rajapakse V, King C, Jacobetz MA, Ross S, Conrads TP, Veenstra TD, Hitt BA, Kawaguchi Y, Johann D, Liotta LA, Crawford HC, Putt ME, Jacks T, Wright CV, Hruban RH, Lowy AM, Tuveson DA, Preinvasive and invasive ductal pancreatic cancer and its early detection in the mouse, Cancer Cell, 4 (2003) 437–450. [PubMed: 14706336]

[15]. Rezen T, Rozman D, Kovacs T, Kovacs P, Sipos A, Bai P, Miko E, The role of bile acids in carcinogenesis, Cell Mol Life Sci, 79 (2022) 243. [PubMed: 35429253]

[16]. Yan N, Yan T, Xia Y, Hao H, Wang G, Gonzalez FJ, The pathophysiological function of non-gastrointestinal farnesoid X receptor, Pharmacol Ther, 226 (2021) 107867. [PubMed: 33895191]

[17]. Zhou M, Wang D, Li X, Cao Y, Yi C, Wiredu Ocansey DK, Zhou Y, Mao F, Farnesoid-X receptor as a therapeutic target for inflammatory bowel disease and colorectal cancer, Front Pharmacol, 13 (2022) 1016836. [PubMed: 36278234]

[18]. Attia YM, Tawfiq RA, Ali AA, Elmazar MM, The FXR Agonist, Obeticholic Acid, Suppresses HCC Proliferation & Metastasis: Role of IL-6/STAT3 Signalling Pathway, Sci Rep, 7 (2017) 12502. [PubMed: 28970500]

[19]. Barone I, Vircillo V, Giordano C, Gelsomino L, Gyorffy B, Tarallo R, Rinaldi A, Bruno G, Caruso A, Romeo F, Bonofiglio D, Ando S, Catalano S, Activation of Farnesoid X Receptor

impairs the tumor-promoting function of breast cancer-associated fibroblasts, Cancer Lett, 437 (2018) 89–99. [PubMed: 30176263]

[20]. Girisa S, Henamayee S, Parama D, Rana V, Dutta U, Kunnumakkara AB, Targeting Farnesoid X receptor (FXR) for developing novel therapeutics against cancer, Mol Biomed, 2 (2021) 21. [PubMed: 35006466]

[21]. Gal E, Vereb Z, Kemeny L, Rakk D, Szekeres A, Becskehazi E, Tiszlavicz L, Takacs T, Czako L, Hegyi P, Venglovecz V, Bile accelerates carcinogenic processes in pancreatic ductal adenocarcinoma cells through the overexpression of MUC4, Sci Rep, 10 (2020) 22088. [PubMed: 33328627]

[22]. Giaginis C, Koutsounas I, Alexandrou P, Zizi-Serbetzoglou A, Patsouris E, Kouraklis G, Theocharis S, Elevated Farnesoid X Receptor (FXR) and Retinoid X Receptors (RXRs) expression is associated with less tumor aggressiveness and favourable prognosis in patients with pancreatic adenocarcinoma, Neoplasma, 62 (2015) 332–341. [PubMed: 25591600]

[23]. Sun L, Cai J, Gonzalez FJ, The role of farnesoid X receptor in metabolic diseases, and gastrointestinal and liver cancer, Nat Rev Gastroenterol Hepatol, 18 (2021) 335–347. [PubMed: 33568795]

[24]. Ignacio Barrasa J, Olmo N, Perez-Ramos P, Santiago-Gomez A, Lecona E, Turnay J, Antonia Lizarbe M, Deoxycholic and chenodeoxycholic bile acids induce apoptosis via oxidative stress in human colon adenocarcinoma cells, Apoptosis, 16 (2011) 1054–1067. [PubMed: 21789651]

[25]. Shrader HR, Miller AM, Tomanek-Chalkley A, McCarthy A, Coleman KL, Ear PH, Mangalam AK, Salem AK, Chan CHF, Effect of bacterial contamination in bile on pancreatic cancer cell survival, Surgery, (2020).

[26]. Wu Z, Lu Y, Wang B, Liu C, Wang ZR, Effects of bile acids on proliferation and ultrastructural alteration of pancreatic cancer cell lines, World J Gastroenterol, 9 (2003) 2759–2763. [PubMed: 14669328]

[27]. Zheng Y, Sun W, Wang Z, Liu J, Shan C, He C, Li B, Hu X, Zhu W, Liu L, Lan F, Jiang C, Zhao C, Li X, Sun N, Activation of Pancreatic Acinar FXR Protects against Pancreatitis via Osgin1-Mediated Restoration of Efficient Autophagy, Research (Wash D C), 2022 (2022) 9784081. [PubMed: 36405253]

[28]. Booth DM, Murphy JA, Mukherjee R, Awais M, Neoptolemos JP, Gerasimenko OV, Tepikin AV, Petersen OH, Sutton R, Criddle DN, Reactive oxygen species induced by bile acid induce apoptosis and protect against necrosis in pancreatic acinar cells, Gastroenterology, 140 (2011) 2116–2125. [PubMed: 21354148]

[29]. Tran QT, Tran VH, Sendler M, Doller J, Wiese M, Bolsmann R, Wilden A, Glaubitz J, Modenbach JM, Thiel FG, de Freitas Chama LL, Weiss FU, Lerch MM, Aghdassi AA, Role of Bile Acids and Bile Salts in Acute Pancreatitis: From the Experimental to Clinical Studies, Pancreas, 50 (2021) 3–11. [PubMed: 33370017]

[30]. Gnerre C, Blattler S, Kaufmann MR, Looser R, Meyer UA, Regulation of CYP3A4 by the bile acid receptor FXR: evidence for functional binding sites in the CYP3A4 gene, Pharmacogenetics, 14 (2004) 635–645. [PubMed: 15454728]

[31]. Lee JM, Wagner M, Xiao R, Kim KH, Feng D, Lazar MA, Moore DD, Nutrient-sensing nuclear receptors coordinate autophagy, Nature, 516 (2014) 112–115. [PubMed: 25383539]

[32]. Seok S, Fu T, Choi SE, Li Y, Zhu R, Kumar S, Sun X, Yoon G, Kang Y, Zhong W, Ma J, Kemper B, Kemper JK, Transcriptional regulation of autophagy by an FXR-CREB axis, Nature, 516 (2014) 108–111. [PubMed: 25383523]

[33]. Zhang Z, Guo M, Zhao S, Xu W, Shao J, Zhang F, Wu L, Lu Y, Zheng S, The update on transcriptional regulation of autophagy in normal and pathologic cells: A novel therapeutic target, Biomed Pharmacother, 74 (2015) 17–29. [PubMed: 26349958]

[34]. Zhou X, Xie L, Bergmann F, Endris V, Strobel O, Buchler MW, Kroemer G, Hackert T, Fortunato F, The bile acid receptor FXR attenuates acinar cell autophagy in chronic pancreatitis, Cell Death Discov, 3 (2017) 17027. [PubMed: 28660075]

[35]. Li Y, Jadhav K, Zhang Y, Bile acid receptors in non-alcoholic fatty liver disease, Biochem Pharmacol, 86 (2013) 1517–1524. [PubMed: 23988487]

[36]. Xia L, Xu Z, Zhou X, Bergmann F, Grabe N, Buchler MW, Neoptolemos JP, Hackert T, Kroemer G, Fortunato F, Impaired autophagy increases susceptibility to endotoxin-induced chronic pancreatitis, Cell Death Dis, 11 (2020) 889. [PubMed: 33087696]

[37]. Xie L, Xia L, Klaiber U, Sachsenmaier M, Hinz U, Bergmann F, Strobel O, Buchler MW, Neoptolemos JP, Fortunato F, Hackert T, Effects of neoadjuvant FOLFIRINOX and gemcitabine-based chemotherapy on cancer cell survival and death in patients with pancreatic ductal adenocarcinoma, Oncotarget, 10 (2019) 7276–7287. [PubMed: 31921387]

[38]. Sinal CJ, Tohkin M, Miyata M, Ward JM, Lambert G, Gonzalez FJ, Targeted disruption of the nuclear receptor FXR/BAR impairs bile acid and lipid homeostasis, Cell, 102 (2000) 731–744. [PubMed: 11030617]

[39]. Kawaguchi Y, Cooper B, Gannon M, Ray M, MacDonald RJ, Wright CV, The role of the transcriptional regulator Ptf1a in converting intestinal to pancreatic progenitors, Nat Genet, 32 (2002) 128–134. [PubMed: 12185368]

[40]. Fortunato F, Burgers H, Bergmann F, Rieger P, Buchler MW, Kroemer G, Werner J, Impaired autolysosome formation correlates with Lamp-2 depletion: role of apoptosis, autophagy, and necrosis in pancreatitis, Gastroenterology, 137 (2009) 350–360, 360 e351–355. [PubMed: 19362087]

[41]. Gu H, Fortunato F, Bergmann F, Buchler MW, Whitcomb DC, Werner J, Alcohol exacerbates LPS-induced fibrosis in subclinical acute pancreatitis, Am J Pathol, 183 (2013) 1508–1517. [PubMed: 24091223]

[42]. Kosar K, Cornuet P, Singh S, Liu S, Nejak-Bowen K, The Thyromimetic Sobetirome (GC-1) Alters Bile Acid Metabolism in a Mouse Model of Hepatic Cholestasis, Am J Pathol, 190 (2020) 1006–1017. [PubMed: 32205094]

[43]. Menz A, Bauer R, Kluth M, Von Bargen CM, Gorbokon N, Viehweger F, Lennartz M, Volkl C, Fraune C, Uhlig R, Hube-Magg C, De Wispelaere N, Minner S, Sauter G, Kind S, Simon R, Burandt E, Clauditz T, Lebok P, Jacobsen F, Steurer S, Wilczak W, Krech T, Marx AH, Bernreuther C, Diagnostic and prognostic impact of cytokeratin 19 expression analysis in human tumors: a tissue microarray study of 13,172 tumors, Hum Pathol, 115 (2021) 19–36. [PubMed: 34102222]

[44]. Zheng YF, Sun WR, Wang ZY, Liu JY, Shan C, He CX, Li BR, Hu X, Zhu WJ, Liu LY, Lan F, Jiang CT, Zhao C, Li XB, Sun N, Activation of Pancreatic Acinar FXR Protects against Pancreatitis via Osgin1-Mediated Restoration of Efficient Autophagy, Research-China, 2022 (2022).

[45]. Guerra C, Barbacid M, Genetically engineered mouse models of pancreatic adenocarcinoma, Mol Oncol, 7 (2013) 232–247. [PubMed: 23506980]

[46]. Antonucci L, Fagman JB, Kim JY, Todoric J, Gukovsky I, Mackey M, Ellisman MH, Karin M, Basal autophagy maintains pancreatic acinar cell homeostasis and protein synthesis and prevents ER stress, Proc Natl Acad Sci U S A, 112 (2015) E6166–6174. [PubMed: 26512112]

[47]. Diakopoulos KN, Lesina M, Wormann S, Song L, Aichler M, Schild L, Artati A, Romisch-Margl W, Wartmann T, Fischer R, Kabiri Y, Zischka H, Halangk W, Demir IE, Pilsak C, Walch A, Mantzoros CS, Steiner JM, Erkan M, Schmid RM, Witt H, Adamski J, Algul H, Impaired autophagy induces chronic atrophic pancreatitis in mice via sex- and nutrition-dependent processes, Gastroenterology, 148 (2015) 626–638 e617. [PubMed: 25497209]

[48]. Kang R, Loux T, Tang D, Schapiro NE, Vernon P, Livesey KM, Krasinskas A, Lotze MT, Zeh HJ 3rd, The expression of the receptor for advanced glycation endproducts (RAGE) is permissive for early pancreatic neoplasia, Proc Natl Acad Sci U S A, 109 (2012) 7031–7036. [PubMed: 22509024]

[49]. Jones S, Zhang X, Parsons DW, Lin JC, Leary RJ, Angenendt P, Mankoo P, Carter H, Kamiyama H, Jimeno A, Hong SM, Fu B, Lin MT, Calhoun ES, Kamiyama M, Walter K, Nikolskaya T, Nikolsky Y, Hartigan J, Smith DR, Hidalgo M, Leach SD, Klein AP, Jaffee EM, Goggins M, Maitra A, Iacobuzio-Donahue C, Eshleman JR, Kern SE, Hruban RH, Karchin R, Papadopoulos N, Parmigiani G, Vogelstein B, Velculescu VE, Kinzler KW, Core signaling pathways in human pancreatic cancers revealed by global genomic analyses, Science, 321 (2008) 1801–1806. [PubMed: 18772397]

[50]. Lee JY, Lee KT, Lee JK, Lee KH, Jang KT, Heo JS, Choi SH, Kim Y, Rhee JC, Farnesoid X receptor, overexpressed in pancreatic cancer with lymph node metastasis promotes cell migration and invasion, Br J Cancer, 104 (2011) 1027–1037. [PubMed: 21364590]

[51]. Chen XL, Xie KX, Yang ZL, Yuan LW, Expression of FXR and HRG and their clinicopathological significance in benign and malignant pancreatic lesions, Int J Clin Exp Pathol, 12 (2019) 2111–2120. [PubMed: 31934033]

[52]. Yang F, Huang X, Yi T, Yen Y, Moore DD, Huang W, Spontaneous development of liver tumors in the absence of the bile acid receptor farnesoid X receptor, Cancer Res, 67 (2007) 863–867. [PubMed: 17283114]

[53]. Distler M, Aust D, Weitz J, Pilarsky C, Grutzmann R, Precursor lesions for sporadic pancreatic cancer: PanIN, IPMN, and MCN, Biomed Res Int, 2014 (2014) 474905. [PubMed: 24783207]

[54]. Bryant KL, Stalnecker CA, Zeitouni D, Klomp JE, Peng S, Tikunov AP, Gunda V, Pierobon M, Waters AM, George SD, Tomar G, Papke B, Hobbs GA, Yan L, Hayes TK, Diehl JN, Goode GD, Chaika NV, Wang Y, Zhang GF, Witkiewicz AK, Knudsen ES, Petricoin EF 3rd, Singh PK, Macdonald JM, Tran NL, Lyssiotis CA, Ying H, Kimmelman AC, Cox AD, Der CJ, Combination of ERK and autophagy inhibition as a treatment approach for pancreatic cancer, Nat Med, 25 (2019) 628–640. [PubMed: 30833752]

[55]. Seton-Rogers S, Eliminating protective autophagy in KRAS-mutant cancers, Nat Rev Cancer, 19 (2019) 247. [PubMed: 30936466]

[56]. Gukovskaya AS, Gukovsky I, Algul H, Habtezion A, Autophagy, Inflammation, and Immune Dysfunction in the Pathogenesis of Pancreatitis, Gastroenterology, 153 (2017) 1212–1226. [PubMed: 28918190]

[57]. Gu H, Werner J, Bergmann F, Whitcomb DC, Buchler MW, Fortunato F, Necro-inflammatory response of pancreatic acinar cells in the pathogenesis of acute alcoholic pancreatitis, Cell Death Dis, 4 (2013) e816. [PubMed: 24091659]

[58]. Kitajima S, Thummalapalli R, Barbie DA, Inflammation as a driver and vulnerability of KRAS mediated oncogenesis, Semin Cell Dev Biol, 58 (2016) 127–135. [PubMed: 27297136]

[59]. Giroux V, Rustgi AK, Metaplasia: tissue injury adaptation and a precursor to the dysplasia-cancer sequence, Nat Rev Cancer, 17 (2017) 594–604. [PubMed: 28860646]

Highlights

- Bile acids have been correlated with poor survival in metastatic PDAC patients.
- Bile acids activate pancreatic FXR *in vitro* and *in vivo*.
- FXR is highly activated in chemo-naïve and neoadjuvant human PDAC tissue.
- FXR activation by BAs reduce pancreatic precancerous lesions in the KC mouse model.
- Loss of FXR eliminates the reduction of pancreatic precancerous lesions by BAs
- FXR is a potential tumor suppressor in PDAC.

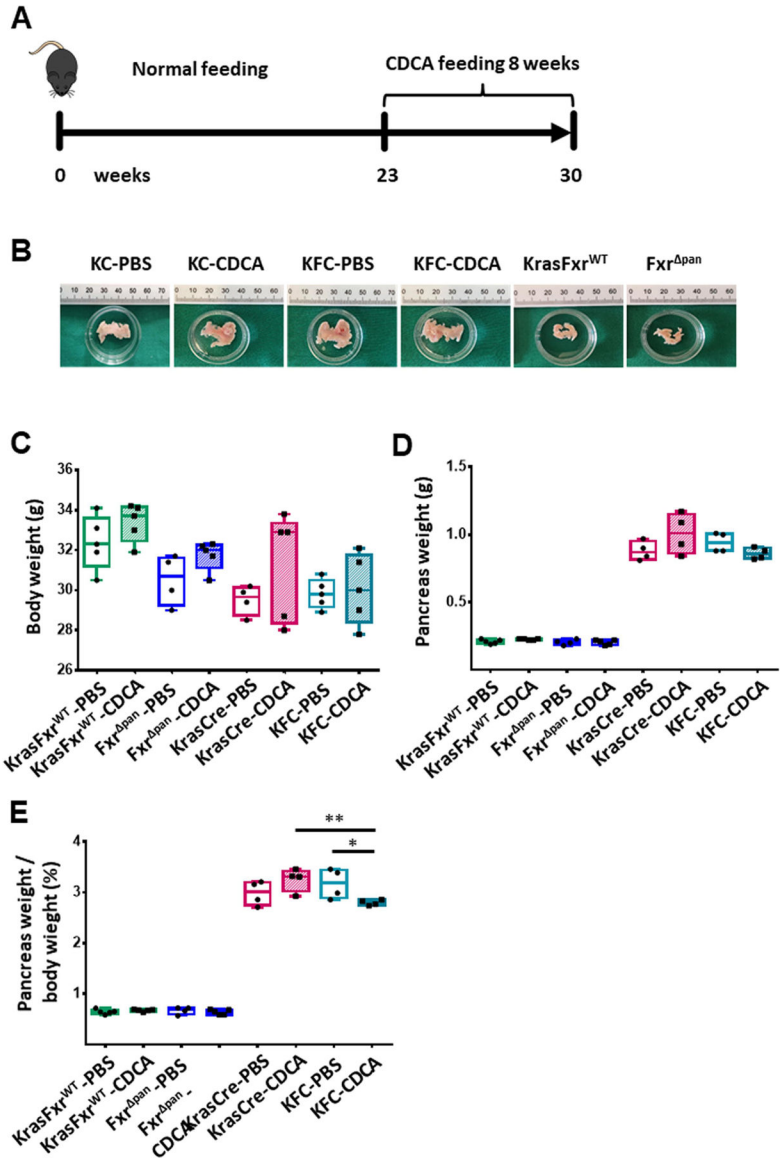

Figure 1. General physiological properties of KC and KFC mice.

(A) Protocol for breeding and CDCA feeding in KC and KFC mice. **(B)** Representative pancreas images for KC, KFC, *Fxr*^{WT}, and *Fxr*$^{\Delta pan}$ mice. **(C)** Body weights of 30-week-old KC and KFC mice with normal and CDCA feeding; plotted data are means ± SEM across five mice per group. **(D)** Pancreas weights of 30-week-old KC and KFC mice with normal and CDCA feeding; plotted data are means ± SEM across five mice per group. **(E)** Pancreas weight to body weight ratios of 30-week-old KC and KFC mice with normal and CDCA feeding; plotted data are means ± SEM across five mice per group.

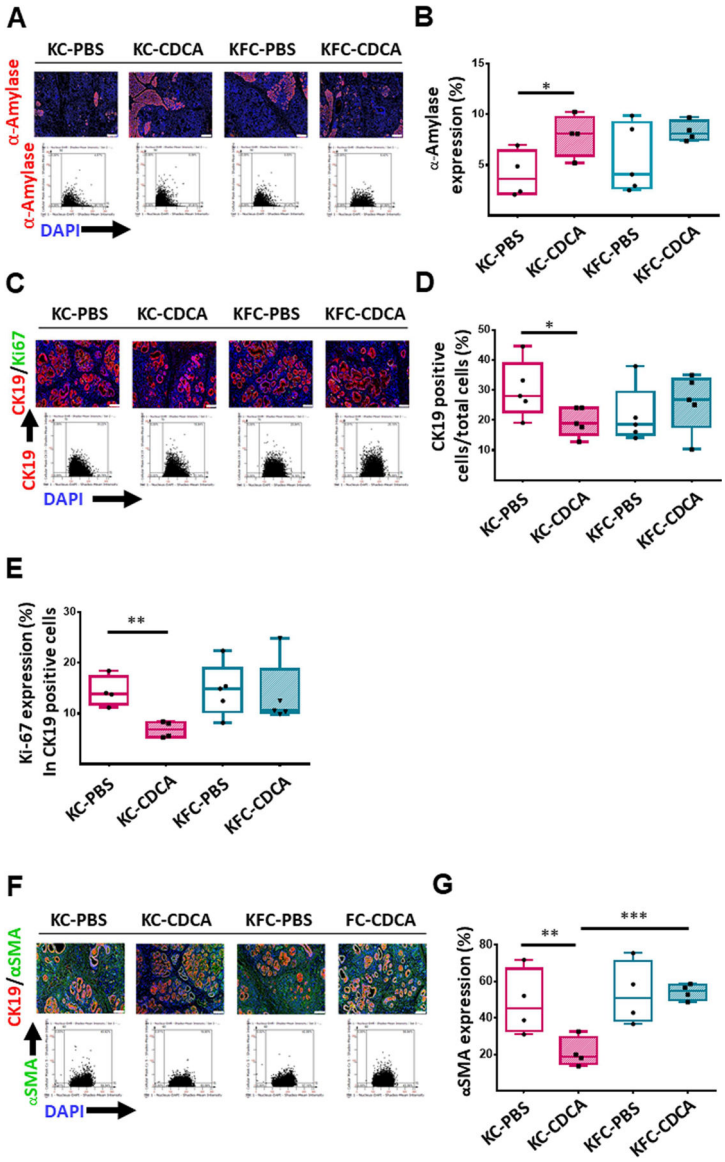

Figure 2. Functional properties of KC and KFC tissues.

(A) Representative IF images (20× objective; scale bar = 200 μm) of pancreatic tissue stained for α-amylase (red) and 4′,6-diamidino-2-phenylindole (DAPI; blue) and fluorescence-activated cell sorting (FACS)-like scattergrams of DAPI and α-amylase quantities in the images. **(B)** α-amylase expression level determined by FACS-like IF quantitation; expression (in %) was plotted as means ± SEM for each group (n = 5). **(C)** Representative IF images (20× objective; scale bar = 200 μm) of pancreatic tissues stained for CK19 (red), Ki67 (green), and DAPI (blue) and FACS-like scattergrams of DAPI, CK19, and Ki67 quantities in the images, and their expression (in %). **(D)** CK19-positive cell proportions as determined by FACS-like IF quantitation plotted as means ± SEM for each group (n = 5). **(E)** Ki67-positive cell proportions in CK19 cells, determined by FACS-like IF quantitation via colocalization analysis, and % expression plotted as means ± SEM for each group (n = 5). **(F)** Representative IF images (20× objective; scale bar = 200 μm)

of pancreatic tissues stained for CK19 and αSMA and FACS-like scattergrams of CK19 and αSMA quantities in the images. **(G)** αSMA-positive cell proportions determined by FACS-like IF quantitation plotted as means ± SEM for each group (n = 5). *, $p < 0.05$; **, $p < 0.01$.

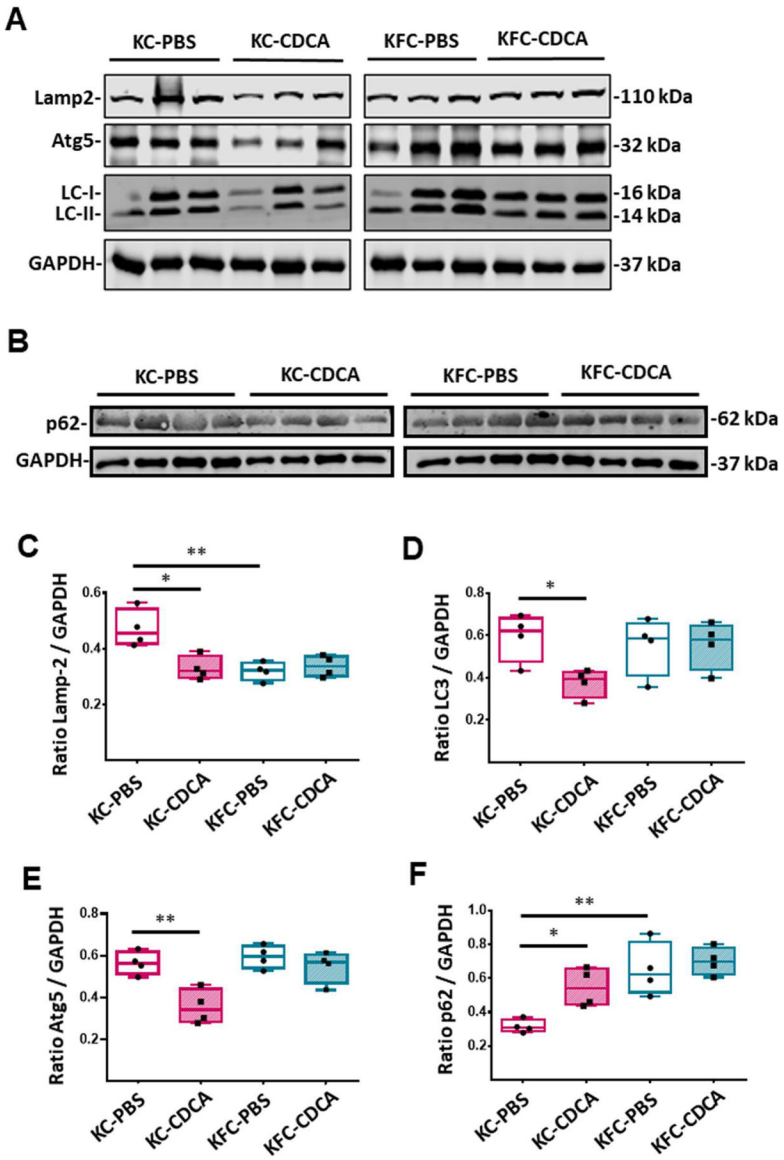

Figure 3. Reduced pancreatic autophagy activity after exposure of mice with intact FXR to CDCA.

(A) Representative immunoblot images of LAMP2, ATG5, LC3, and glyceraldehyde 3-phosphate dehydrogenase (GAPDH; loading control). **(B)** Representative immunoblot images of SQSTM1 (p62) and glyceraldehyde 3-phosphate dehydrogenase (GAPDH; loading control). The protein bands with molecular masses are indicated. Normalized to **(C)** LAMP2, **(D)** LC3, **(E)** ATG5 and **(F)** p62 values plotted as means ± SEM across four animals per group. *, $p < 0.05$; **, $p < 0.01$.

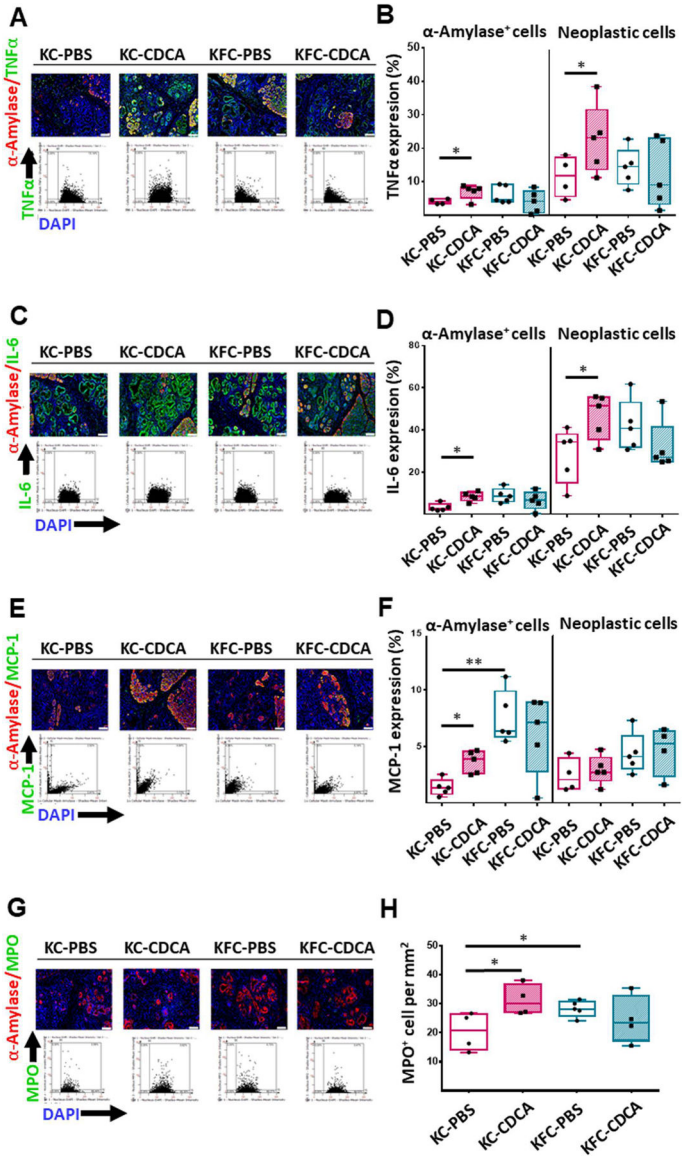

Figure 4. Enhanced pro-inflammatory response in KC mice after BA feeding.

(A) Representative IF colocalization images (20× objective; scale bar = 100 μm) stained for α-amylase (red), TNFα (green), and DAPI (blue) and FACS-like scattergrams. **(B)** IF and FACS-like TNFα quantitation in acinar and neoplastic cells from KC and KFC mice pancreata and its % expression plotted as means ± SEM (n = 4–5 per group). **(C)** Representative IF colocalization images (20× objective; scale bar = 100 μm) stained for α-amylase (red), IL-6 (green), and DAPI (blue) and FACS-like scattergrams. **(D)** IF and FACS-like IL-6 quantitation in acinar and neoplastic cells from KC and KFC mice and its % expression plotted as means ± SEM (n = 4–5 per group). **(E)** Representative IF colocalization images (20× objective; scale bar = 100 μm) stained for α-amylase (red), MCP-1 (green), and DAPI (blue) and FACS-like scattergrams. **(F)** IF and FACS-like MCP-1 quantitation in acinar and neoplastic cells from KC and KFC mice pancreata and its % expression plotted as means ± SEM (n = 4–5 per group). **(G)** Representative IF

colocalization images (20× objective; scale bar = 100 μm) stained for CK19 (red), MPO (green), and DAPI (blue) and FACS-like scattergrams. **(H)** IF and FACS-like quantitation of MPO-positive cells per mm^2 for KC and KFC mice and % expression plotted as means ± SEM (n = 4–5 per group). *, $p < 0.05$; **, $p < 0.01$; ***, $p < 0.001$.

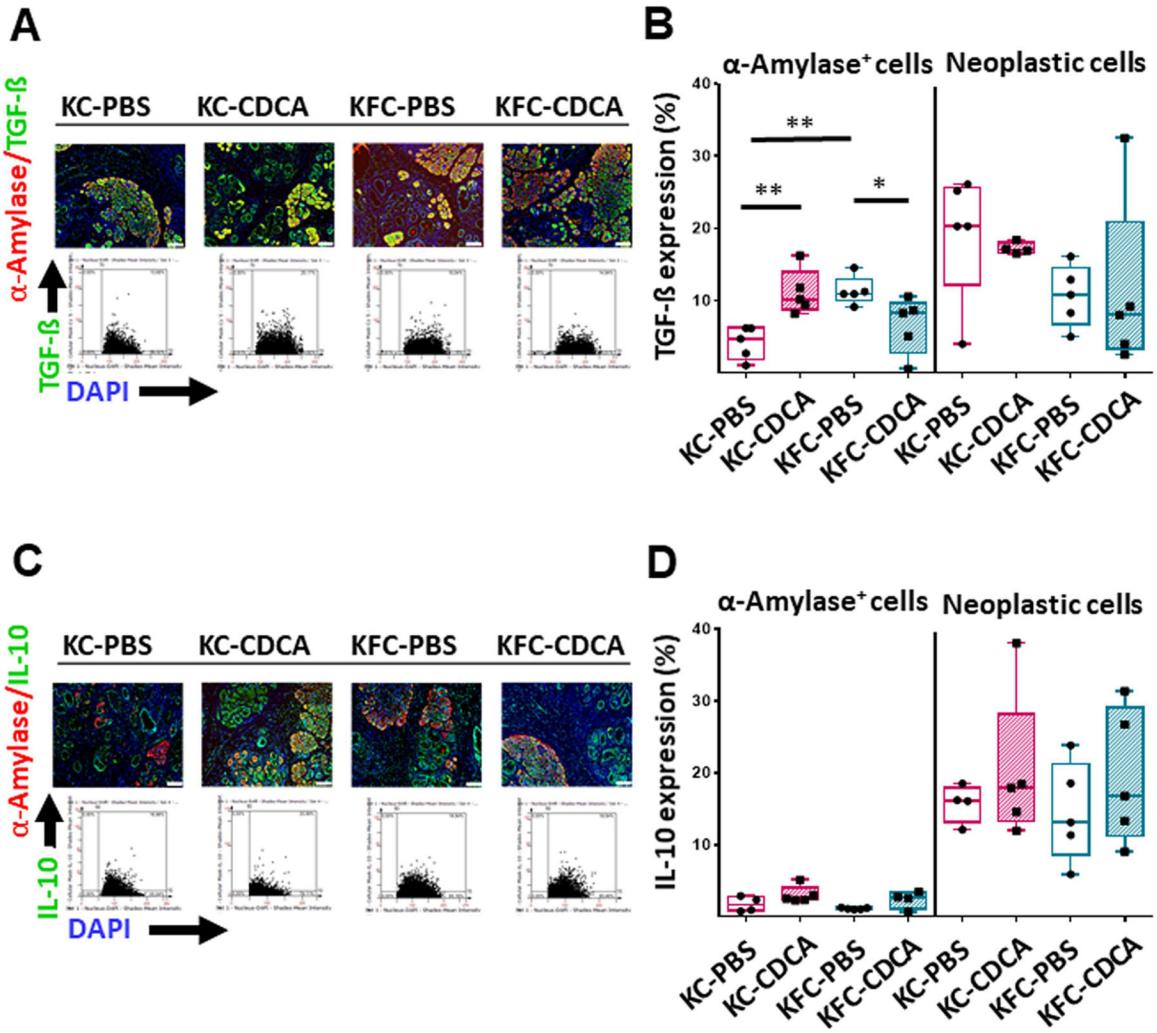

Figure 5. Enhanced anti-inflammatory response in KC mice after BA feeding.

(A) Representative IF colocalization images (20× objective; scale bar = 100 μm) stained for α-amylase (red), TGFβ (green), and DAPI (blue) and FACS-like scattergrams. **(B)** IF and FACS-like TGFβ quantitation in acinar and neoplastic cells from KC and KFC mice pancreata and its % expression plotted as means ± SEM (n = 4–5 per group). **(C)** Representative IF colocalization images (20× objective; scale bar = 100 μm) stained for α-amylase (red), IL6 (green), and DAPI (blue) and FACS-like scattergrams. **(D)** IF and FACS-like IL10 quantitation in acinar and neoplastic cells from KC and KFC mice pancreata and its % expression plotted as means ± SEM (n = 4–5 per group). *, $p < 0.05$.

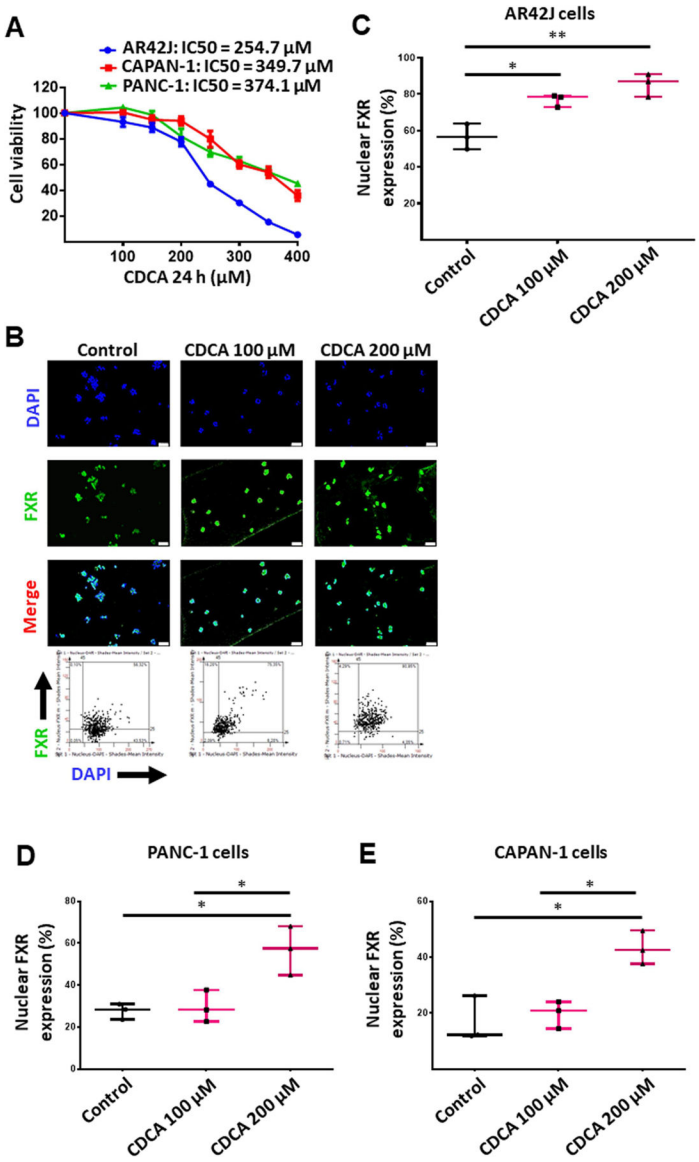

Figure 6. Nuclear FXR activation by BAs in vitro.

(A) MTT assay showing CDCA cytotoxicity in the AR42J (IC50 = 254.7 μM), Capan-1 (IC50 = 349.7 μM), and Panc-1 (IC50 = 374.1 μM) pancreatic tumor cell lines. **(B)** Representative IF images (20× objective; scale bar = 50 μm) stained for FXR (green) and DAPI (blue) and FACS-like scattergrams. **(C)** Nuclear FXR expression in AR42J cells determined by FACS-like IF quantitation, plotted as means ± SEM (repeated thrice). (D) Nuclear FXR expression in PANC-1 cells determined by FACS-like IF quantitation, plotted as means ± SEM (repeated thrice). **(E)** Nuclear FXR expression in CAPAN-1 cells determined by FACS-like IF quantitation, plotted as means ± SEM (repeated triplicates). *, $p < 0.05$; **, $p < 0.01$.

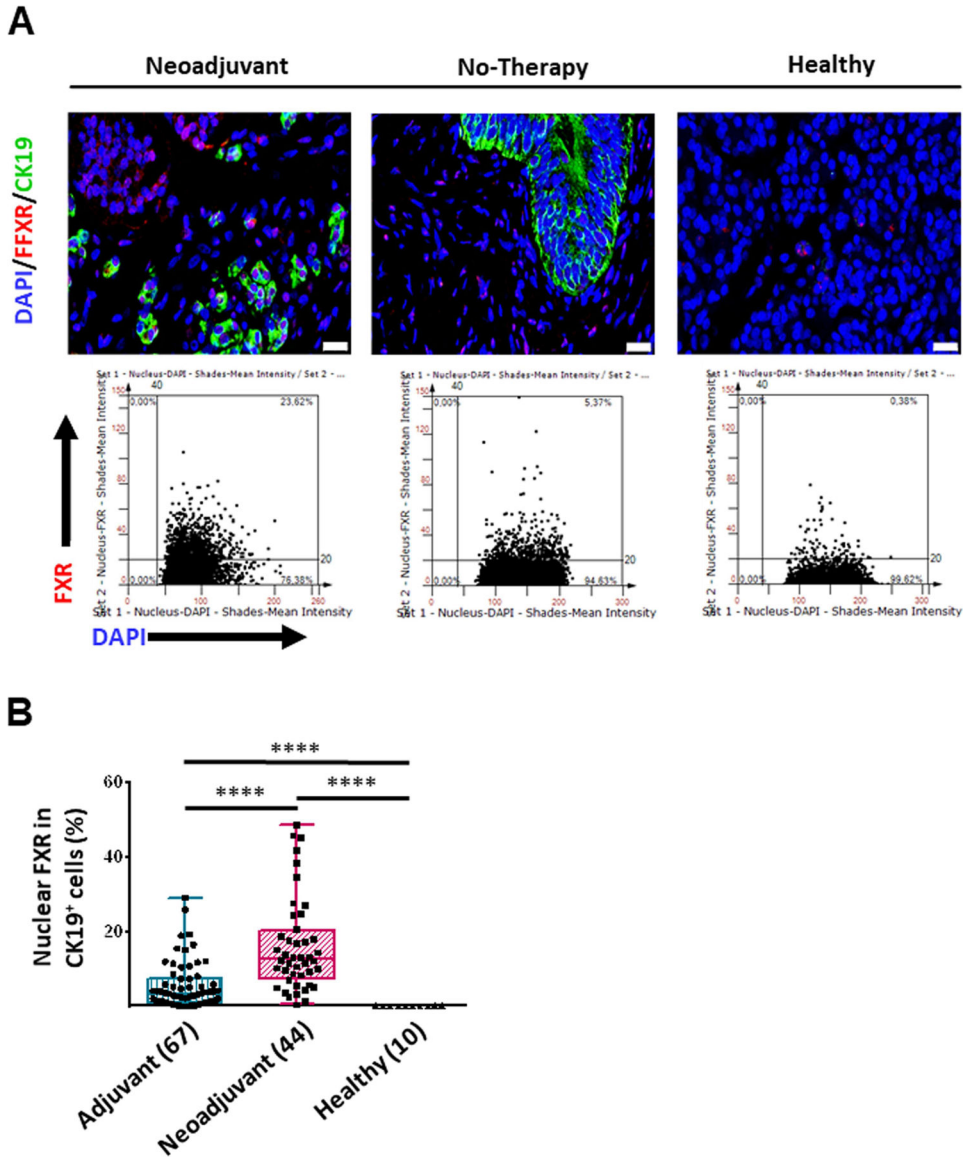

Figure 7. Pancreatic BA receptor FXR expression is highly activated in pancreatic cancer patients.

(A) Representative IF colocalization images (20× objective; scale bar = 20 μm) stained for FXR (red), CK19 (green), and DAPI (blue) and FACS-like scattergrams. **(B)** IF and FACS-like quantitation of nuclear FXR in CK19 cells in pancreatic tissue from healthy donors (n = 9), chemo-naïve adjuvant patients (n = 9), and neoadjuvant patients (n = 18); nuclear FXR and CK19 co-expression (in %) is plotted as means ± SEM. **, $p < 0.01$; ***, $p < 0.001$; ****, $p < 0.0001$.